In Vivo Assembly of Photosystem I-Hydrogenase Chimera for In Vitro PhotoH$_2$ Production

Panpan Wang, Anna Frank, Jens Appel, Marko Boehm, Nadine Strabel,
Marc M. Nowaczyk,* Wolfgang Schuhmann,* Felipe Conzuelo,* and Kirstin Gutekunst*

Photosynthetic hydrogen (photoH$_2$) production is an elegant approach to storing solar energy. The most efficient strategy is to couple the hydrogen-producing enzyme, the hydrogenase (H$_2$ase), directly to photosystem I (PSI), which is a light-driven nanomachine found in photosynthetic organisms. PSI–H$_2$ase fusions have been tested in vivo and in vitro. Both approaches have each their specific advantages and drawbacks. Here, a system to combine both approaches by assembling PSI–H$_2$ase fusions in vivo for in vitro photoH$_2$ production is established. For this, cyanobacterial PSI–H$_2$ase fusion mutants are generated and characterized concerning photoH$_2$ production in vivo. The chimeric protein is purified and embedded in a redox polymer on an electrode where it successfully produces photoH$_2$ in vitro. The combination of in vivo and in vitro processes comes along with reciprocal benefits. The in vivo assembly ensures that the chimeric protein is fully functional and suited for the fabrication of bioelectrodes in vitro. At the same time, the photoelectrochemical in vitro characterization now permits to analyze the assemblies in detail. This will open avenues to optimize in vivo and in vitro approaches for photoH$_2$ production in a target-oriented manner in the future.

1. Introduction

Hydrogen production directly coupled to photosynthesis belongs to the most sustainable ways of solar energy conservation. Green algae and cyanobacteria can do just this for a few minutes in transition states between dark to light conditions. They utilize light-excited electrons to transiently store a surplus of energy as photoH$_2$ at the onset of photosynthesis after a period of dark adaptation. However, this hydrogen is subsequently consumed again by the cells. The algal and cyanobacterial hydrogenases that catalyze the production and consumption of hydrogen are oxygen sensitive. As soon as photosynthesis operates at full capacity, molecular oxygen accumulates due to water splitting at photosystem II (PSII) and inactivates hydrogen production. The amount of photoH$_2$ that natural cyanobacteria and algae produce does not suffice for biotechnological approaches. Therefore, several strategies have been established to enhance and prolong in vivo photoH$_2$ production via genetic manipulations and modified culture conditions.[1] The most efficient and direct approach is to fuse the hydrogenase to PSI genetically. The light-induced charge separation in PSI unleashes an electron transfer pathway within PSI, which finally reduces the terminal 4Fe4S cluster F$_B$. In natural cyanobacterial and algal strains, F$_B$ transfers electrons to the soluble electron carrier ferredoxin, which donates electrons to a plethora of metabolic reactions. The fusion of a hydrogenase to PSI aims to harness these low potential electrons from F$_B$. This was recently accomplished in vivo in the green alga *Chlamydomonas rheinhardtii* and the cyanobacterium *Synechocystis* sp. PCC 6803.[2]

P. Wang, W. Schuhmann
Analytical Chemistry–Center for Electrochemical Sciences (CES)
Faculty of Chemistry and Biochemistry
Ruhr University Bochum
Universitätsstr. 150, D-44780 Bochum, Germany
E-mail: wolfgang.schuhmann@rub.de

The ORCID identification number(s) for the author(s) of this article can be found under https://doi.org/10.1002/aenm.202203232.

[+]Present address: Biochemistry, Institute of Biosciences, University of Rostock, Albert-Einstein-Str. 3, 18059 Rostock, Germany

A. Frank, N. Strabel, M. M. Nowaczyk[+]
Plant Biochemistry–Molecular Mechanisms of Photosynthesis
Faculty of Biology and Biotechnology
Ruhr University Bochum
Universitätsstr. 150, D-44780 Bochum, Germany
E-mail: marc.m.nowaczyk@rub.de

J. Appel, M. Boehm, K. Gutekunst
Molecular Plant Physiology, Bioenergetics in Photoautotrophs
University Kassel
Heinrich-Plett-Straße 40, D-34132 Kassel, Germany
E-mail: kirstin.gutekunst@uni-kassel.de

F. Conzuelo
Instituto de Tecnologia Química e Biológica António Xavier
Universidade Nova de Lisboa
Av. Da República, 2780-157 Oeiras, Portugal
E-mail: felipe.conzuelo@itqb.unl.pt

Table 1. Advantages, drawbacks, and challenges of PSI–H$_2$ase in vivo and in vitro systems.

	PSI–H$_2$ase in vivo	PSI–H$_2$ase in vitro
Complex assembly	Cheap, fast, and nonlaborious	Laborious
Complex stability	High	Low
Competition by metabolic reactions	Present	Absent
Maintenance and repair	Present	Absent
Electronic short circuits between donor and acceptor side of PSI	Absent (barrier function of thylakoid membranes)	Present
Charge recombination within PSI	Present	Present
Theoretically achievable electron transfer rates through PSI–H$_2$ase complex	Limited by complexes of photosynthetic electron transfer chain	High (PSI electron transfer throughput of in vitro systems can be about five times faster than for in vivo systems)[5]
Protection from oxygen	Challenging	Possible by the implementation of two half-cells
Characterization of electron transfer in PSI–H$_2$ase complexes	Possible, but overlayed by competing metabolic reactions	Possible
Long-term viability	Not an issue	An issue

Both mutant strains produce photoH$_2$ for several hours under anaerobic conditions in the light. In the cyanobacterial mutant strain, electron transfer rates between PSI and the H$_2$ase are far from the theoretical maximum and require optimization.

The first direct fusions of H$_2$ases to PSI were achieved in vitro by self-assembly of genetically modified and separately purified proteins.[3] These PSI–H$_2$ase complexes successfully produce photoH$_2$ on electrodes upon illumination. By the integration of a molecular wire that directly connects the F$_B$ cluster of PSI and the distal FeS cluster of a H$_2$ase, it was possible to obtain electron transfer rates that exceed those found in the electron transport chain of natural photosynthesis.[4] In vivo and in vitro approaches for photoH$_2$ production have specific advantages, drawbacks, and challenges. A comparison of both approaches provides a deeper understanding of both techniques (**Table 1**).

In vivo systems offer a cheap, fast, and nonlaborious protein complex assembly, including quality control, repair and reproduction and thus enable the longevity of the fusion protein complexes. The price is the presence of competing metabolic reactions that drain the excited electrons from PSI for cell maintenance. However, an ideal PSI–H$_2$ase fusion complex with optimal electron transfer rates that can completely expel competing reactions would lead to cell death. Therefore, a balance between photoH$_2$ production efficiency and metabolism must be found. This puts a limit on the theoretical in vivo efficiency in contrast to in vitro systems. In vitro systems, on the other hand, lack quality control, repair and maintenance, suffer from short operational lifetimes and require laborious complex assembly. However, metabolic reactions that compete for electrons are absent in such systems. In nature, PSI is embedded in thylakoid membranes, which ensures proper orientation of the protein complexes and prevents a direct interaction between the electron donor of P$_{700}$ and the electron acceptor of F$_B$. In vitro systems lack this physical barrier function and are hence challenged by electronic short circuits bypassing PSI, which may be partly due to an improper orientation of PSI complexes relative to the electrode surface or due to the use of electron donors/acceptors freely diffusing in solution.[6] The use of PSI

monolayers, which allow control over the orientation of PSI, was proposed to mitigate these limitations. These monolayers were coupled with redox polymers that ensure efficient electronic communication of PSI with the electrode surface without requiring the presence of electron donors in solution.[7] The potential difference in PSI between P$_{700}^+$ and F$_B^-$ is around 1.0 V upon illumination, which imposes a large driving force for charge recombination both for in vitro and in vivo systems. The most efficient prevention of charge recombination is an efficient electron acceptor of F$_B^-$, which is ideally a hydrogenase. Truly sustainable photoH$_2$ production requires that the electrons are extracted from water oxidation. However, this aim is especially challenging in vivo, as oxygen accumulation from water splitting at PSII inactivates most H$_2$ases. By contrast, in vitro systems can separate water splitting at PSII and hydrogen production at PSI into two half-cells and thereby overcome this hurdle. However, in vitro PSII is particularly unstable due to the absence of a repair mechanism.

Thus, combining in vivo and in vitro approaches results in reciprocal benefits. The nonlaborious in vivo assembly and testing of new chimeric proteins ensures the production of complexes that have the potential of being suitable for in vitro systems as well. On the other hand, low electron transfer rates between PSI and the H$_2$ase are currently the most significant limitation for efficient photoH$_2$ production in cyanobacterial mutant strains. The purification and photoelectrochemical characterization of cyanobacterial PSI–H$_2$ase complexes in vitro will allow the identification of bottlenecks in the absence of metabolic competitors and thereby enable targeted optimization for the design of new fusions. Here we accomplished the in vivo assembly, isolation, and in vitro photoH$_2$ production via a PSI–H$_2$ase chimera as a proof of concept to open a new avenue for reciprocal optimization processes (**Figure 1**). Following this strategy, optimal coupling of redox centers without requiring molecular wires for connecting the FeS clusters of PSI and H$_2$ase is expected. The electron transfer kinetics between the two biomolecules can be maximized in accordance with Marcus' theory, which predicts an exponential decay of the rate constant for electron transfer with an increasing donor-acceptor
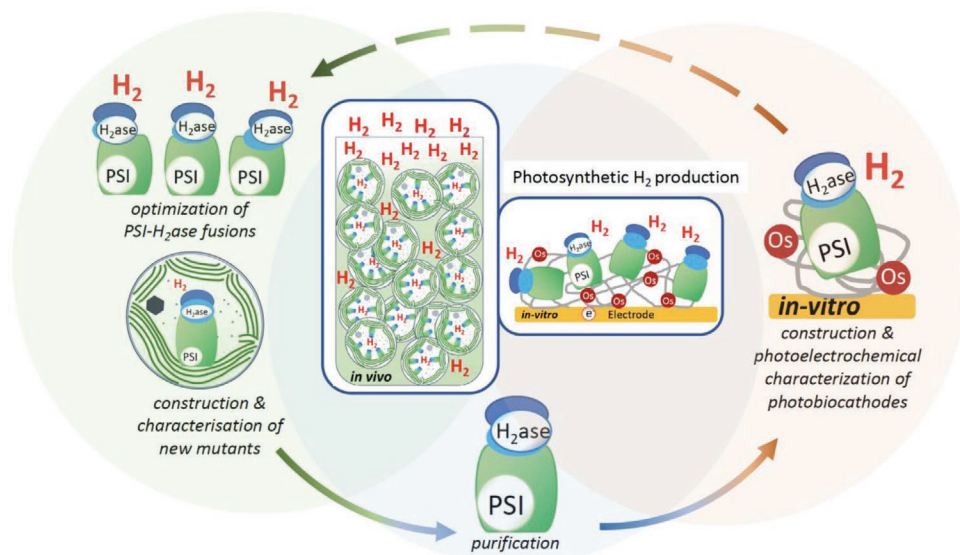
ADVANCED
SCIENCE NEWS
www.advancedsciencenews.com

ADVANCED
ENERGY
MATERIALS
www.advenergymat.de

Figure 1. Workflow of optimization, in vivo assembly, purification, and immobilization of PSI-hydrogenase chimera on electrodes within a redox polymer followed by in vitro photoH$_2$ production. In this study, purification and integration of the active fusions into a photochemical device were accomplished. This allows for further optimization of the fusions in an iterative process as indicated by the dashed arrow.

distance.[8] Consequently, the isolated PSI–H$_2$ase complexes can be integrated within a redox hydrogel for the fabrication of bioelectrodes for in vitro photoH$_2$ production where electronic short circuits between the donor and acceptor side of PSI are prevented to a great extent, independent of the orientation of the complex within the hydrogel film.

2. Results and Discussion

2.1. PSI–H$_2$ase Fusion Complex In Vivo

The in vivo electron transfer rates within the PSI–H$_2$ase fusion complex in the cyanobacterial PsaD–HoxYH strain, in which the hydrogenase subunits HoxYH were fused to the PSI subunit PsaD, are rather poor.[2b] The distance between the FeS clusters of PSI and the hydrogenase is especially critical for an efficient electron transfer. The calculated distance between F$_B$ of PSI and the 4Fe4S cluster of HoxY is between 23 and 45 Å in PsaD–HoxYH, which is above the ideal distance of 14 Å.[2b,9] Therefore, new PSI–H$_2$ase fusion mutants were constructed in the cyanobacterium *Synechocystis* sp. PCC 6803 to possibly shorten the distance between the FeS clusters of PSI and the H$_2$ase. The structure of PSI of *Synechocystis* sp. PCC 6803 has been solved,[10] but the structure of its hydrogenase is not known. Since the cyanobacterial bidirectional hydrogenase is very similar to the soluble hydrogenases of the oxyhydrogen bacteria the structure from *Hydrogenophilus thermoluteolus*[11] was used as a blueprint.

Due to the configuration of the stromal subunits of PSI (PsaC and D) and of the NiFe-hydrogenase subunits HoxYH, it is difficult to get to distances shorter than 14 Å as required when fusing HoxYH to PsaD or into PsaC. This is because the proximal FeS cluster of HoxY is about 30 Å from its N-terminus. In the case of the algal FeFe-hydrogenase this is different. It could be internally fused into a β-turn of PsaC placing its H cluster in

close proximity to F$_B$ and yielding a fusion strain with adequate electron transfer properties.[1,2a]

We used a similar strategy and introduced HoxY into the same β-turn of PsaC using linker lengths between 5 and 18 amino acids at its N- and C-terminus generating three different fusion constructs (PsaC–HoxYH I, II and III; see Figure S1A and Table S1 in the Supporting Information). Estimations of the shortest attainable distances between the FeS clusters were in the range of 10–20 Å in the most favorable configurations. All fusion strains produced an active hydrogenase, the activity was attached to the membrane and the respective fusion proteins were found by immunoblotting (Figures S1B and S2, Supporting Information). This indicates that the overall construction was successful, and allowed proper folding of the PsaC–HoxY fusion protein and its integration into PSI. Note that in all strains the native PsaC is still expressed in large quantities (Figure S2, Supporting Information). However, none of them produced photoH$_2$ (Figure S1C, Supporting Information). Thus, none of the chimeras had a sufficiently short distance between the FeS clusters to allow electron transfer.

Based on these results and the relatively poor electron transfer in the PsaD–HoxYH strain, the best alternative seems to be to fuse HoxY with its C-terminus to PsaE. The proximal FeS cluster is close to the C-terminus and about 8.6 Å from the surface. This distance could be made even shorter when the C-terminus is truncated. Provided a sufficiently long linker is used, HoxY could move into the ferredoxin binding site which is a shallow groove made up of PsaC, D, and E and distances of 14 Å and shorter should be possible.

In the mutant PsaE-16–HoxYH, the C-terminus of HoxY was fused to the N-terminal Gly6 of PsaE with a 16 aa linker (EKSSGSGSESKSTEKS). This linker is known to be flexible and, due to the Lys and Glu residues, should have sufficient solubility.[12] In principle, this linker should enable the HoxY
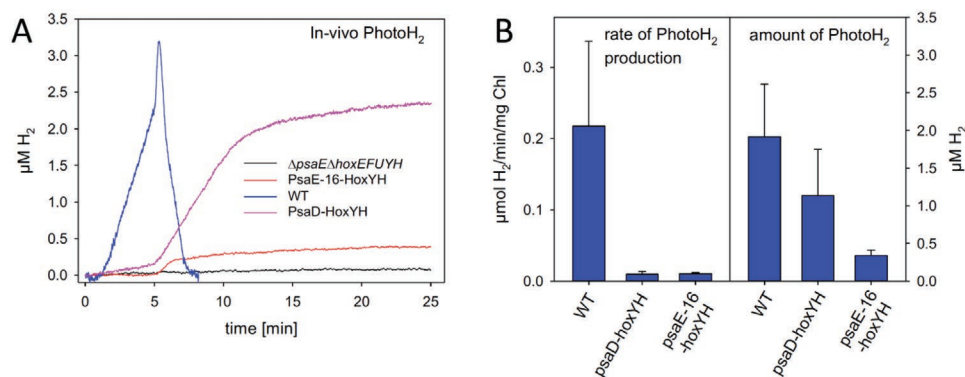
Figure 2. Fermentative H$_2$ production and photoH$_2$ production of WT, $\Delta psaE\Delta hoxEFUYH$, PsaE-16–HoxYH and PsaD–HoxYH. A) Cells were kept under anaerobic, dark conditions for 5 min for fermentative H$_2$ production. Upon illumination, photoH$_2$ production was initiated in the WT, PsaE-16–HoxYH, and PsaD–HoxYH. B) PhotoH$_2$ production rate and amount of photoH$_2$.

subunit to move into the ferredoxin binding site[13] (Figure S3, Supporting Information). Based on our model, the shortest possible distance attainable under these circumstances would be close to 12 Å between the F$_B$ cluster of PsaC and the proximal FeS cluster of HoxY, providing an improved situation in comparison to the previously published PsaD–HoxYH fusion strain.[2b]

Genomic DNA of the mutant was isolated and subjected to southern blotting, which confirmed its segregation (Figure S4, Supporting Information). Hydrogenase activity measurements with reduced methyl viologen as an artificial electron donor proved that HoxYH is correctly assembled and yields an active enzyme in the mutant strain $\Delta psaE\Delta hoxEFUYH/hoxY$-16aa linker-$psaE$-$hoxH$. This strain will be referred to here as PsaE-16–HoxYH (Figure S5A, Supporting Information). Cell fractionation indicated that most of the hydrogenase activity was located in the membrane fraction of the mutant strain (Figure S5B, Supporting Information). The presence of PsaE and the hydrogenase subunits HoxY and HoxH was furthermore assessed by two-dimensional BN-SDS PAGE gels followed by immunoblotting. Solubilized membrane fractions were loaded on a blue native (BN) gel to separate protein complexes (Figure S6A, Supporting Information). The PSI subunit PsaE was mainly detected in the membrane fraction as expected and was modulated in size in the mutant strain due to the attachment of HoxY (Figure S6B, Supporting Information). HoxY was present in the soluble fraction of WT cells. Small amounts of HoxY were also present in the soluble fraction of PsaE-16–HoxYH, which indicates that small amounts of the fusion construct were not integrated into PSI in the thylakoid membrane or might have been lost from the complex upon cell breakage. However, most of the PsaE–HoxY fusion including HoxH was detected in the membrane fraction in PsaE-16–HoxYH (Figure S6C,D, Supporting Information). The protein complexes of the membrane fractions of PsaE-16–HoxYH were subsequently separated under denaturing conditions in the second dimension (Figure S7, Supporting Information). PSI–H$_2$ase fusion seemed to be assembled correctly in the mutant. Therefore, PsaE-16–HoxYH mutant strains were investigated concerning their hydrogen production in vivo (**Figure 2**).

The Synechocystis WT produces hydrogen under anaerobic fermentative conditions in darkness. Upon illumination, these dark-adapted cells utilize excited electrons from the photosynthetic electron transport chain and produce a short burst of photoH$_2$, which is subsequently consumed. The electrons from H$_2$ uptake are fed back into the photosynthetic electron transfer chain. The PsaE-16–HoxYH mutant strain did not produce any fermentative hydrogen. This was expected as the mutant lacks the diaphorase subunits HoxEFU, which are responsible for interacting with the cellular redox partners NAD(P)H and ferredoxin.[14] Upon illumination, PsaE-16–HoxYH produced photoH$_2$. In contrast to the WT, photoH$_2$ was not consumed in the mutant (Figure 2A). This is in line with earlier observations in the PsaD–HoxYH strain and is due to the absence of the diaphorase and the immobility of the hydrogenase in the fusion mutants, which impedes the feeding of electrons back into the photosynthetic electron transfer chain.[2b]

In case of the hydrogenase tethered to the PsaE subunit, optimization is only possible if the accuracy of fit of the protein surfaces and their distribution of charges enables competition with ferredoxin. Despite all theoretical considerations about the folding and orientation of the fused proteins, large uncertainties remain about their real in vivo configuration and the achievable electron transfer rates in the actual PSI–H$_2$ase complexes. To this end, the purification of the complexes for the generation of structural information and especially their photoelectrochemical in vitro analyses in a competition-free environment are indispensable tools. This is because small changes in the binding affinity of the hydrogenase might not be visible in vivo due to the strong competition with ferredoxin but would be more obvious in vitro when comparing the photocurrent of different complexes. To establish a proof of concept and respective workflow (Figure 1) we chose the PsaE-16–HoxYH strain. An additional advantage of this strain is its faster growth compared to PsaD–HoxYH (**Figure 3**). Supplying BG-11 media with ferric ammonium citrate (FAC) after autoclaving lowers the precipitation rate of FAC and thus better meets the iron requirements of the cells and promotes even higher growth rates (Figure 3).

2.2. Isolation and Purification of PSI–H$_2$ase Protein Complexes

Cultivation of the PSI–Hox mutant strain PsaE-16–HoxYH showed optimal cell growth in a 0.4–1 L tempered, gassed glass
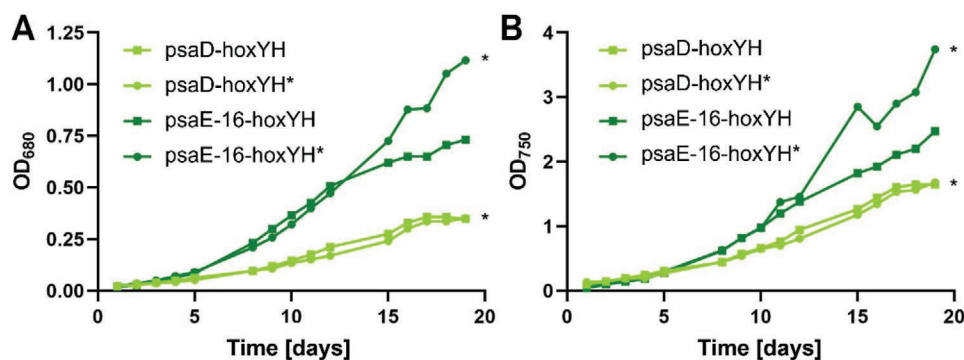
Figure 3. Autotrophic growth of WT, PsaD–HoxYH[2b] and PsaE-16–HoxYH in different BG11 media. Measurement of scatter-free OD_{680} A) and OD_{750} B) over a period of 20 days. Cultures marked with * were grown in BG11 medium supplied with ferric ammonium citrate after autoclaving.

tube system with growth rates similar to the WT and significantly faster than the previously reported PsaD–HoxYH mutant (Figure 3).[2b]

After cell disruption, thylakoid membranes were treated with lauryl dimethyl amine oxide (LDAO) for the extraction of membrane proteins and monomerization of solubilized PSI complexes.[6,15] PSI–Hox fusion constructs could be isolated successfully via hydrophobic interaction chromatography (HIC) (Figure S8, Supporting Information). Despite partial contamination with PSII and phycobilisomes (Figure S9, Supporting Information), PSI was found to be the major protein complex in HIC-purified samples, displaying the characteristic PSI band pattern on denaturing SDS-PAGE (Figure S10A, Supporting Information).

All major PSI subunits could be found and assigned to PsaA/B, PsaC, PsaD, PsaF, and PsaL. The band of native PsaE at a size of 8.3 kDa could be confirmed to be absent in the SDS-PAGE analysis of the HIC-purified PsaE-16–HoxYH samples. Instead, a band at the expected size of around 28 kDa for the PsaE–HoxY fusion was observed. Conclusively, the presence of the fusion subunit HoxY was validated in both isolated constructs via immunodetection with a HoxY protein-specific antibody. In the same way, HoxH, the second subunit of the active H_2ase moiety, which is not fused to any PSI subunit but must attach autonomously to HoxY, was confirmed to be present in the fusion construct (Figure S10B, Supporting Information), verifying the integrity of the PSI–H_2ase complex chimeras. HoxH signals were present as a characteristic double band in immunoblotting analysis, corresponding to the processed (51.1 kDa) and an unprocessed (52.9 kDa) immature form of the subunit.[2b,16]

2.3. In Vitro PhotoH_2 Production

The isolated PSI–HoxYH complexes were immobilized on electrodes for the fabrication of a biophotocathode capable of providing light-induced H_2 evolution. For this, PSI–H_2ase complexes were integrated into a redox polymer matrix, which consisted of an Os-complex-modified poly(vinyl)imidazole polymer (P-Os; see Figure S11, Supporting Information). The redox polymer presents a redox complex with an adjusted potential for providing fast electron transfer with the P_{700} site

at PSI while ensuring a minimum overpotential. As it has been shown before in combination with isolated cyanobacterial PSI, the optimized redox polymer enabled the achievement of benchmark electron transfer rates that even outperform the rates observed in natural photosynthesis.[17]

To confirm the electrical wiring of PSI–HoxYH complexes, P-Os modified electrodes were fabricated by integrating the chimeric complexes into the redox polymer that simultaneously served as immobilization matrix. The photocurrent response was measured in the presence of methyl viologen (MV^{2+}) as free-diffusing electron scavenger in air-equilibrated solutions. As expected, cathodic photocurrents were observed upon illumination of the bioelectrode (Figure S12A, Supporting Information) as a result of the Os complexes in the redox polymer donating electrons for the reduction of photo-oxidized P_{700}^+, while the high-energy electrons exiting PSI at the F_B^- FeS cluster are transferred to MV^{2+}, followed by reduction of O_2 in solution as terminal electron acceptor. Moreover, the presence of the characteristic wave for the redox interconversion of the polymer-bound Os complexes was observed at the end of the experiment (Figure S12B, Supporting Information), confirming adequate stability of the modified electrodes.

Subsequently, the photocurrent response of the modified electrode was investigated in the absence of MV^{2+} and under the exclusion of O_2. Under these conditions, the only possibility for sustained photocurrent generation is the transfer of electrons to the fused H_2ase for the concomitant reduction of protons in solution and H_2 evolution. As summarized in **Figure 4**A, cathodic photocurrents were obtained for electrodes modified with PSI–HoxYH complexes in P-Os at different pH values, confirming the possibility for in vitro light-induced H_2 evolution with the isolated fusion complexes. The highest and most stable photocurrent response over several cycles of illumination was attained at a pH value of 5.5 (Figure 4B). This result is consistent with previous experiments where a H_2ase has been coupled to isolated PSI wired to the electrode surface[7] and was selected as the optimum pH value for subsequent measurements.

To rule out any possible contribution of the redox polymer or the electrode surface to the generation of cathodic photocurrents, a control experiment was performed replacing the PSI–HoxYH complex in the modified electrode with a non-redox active protein, i.e., bovine serum albumin (BSA). In this
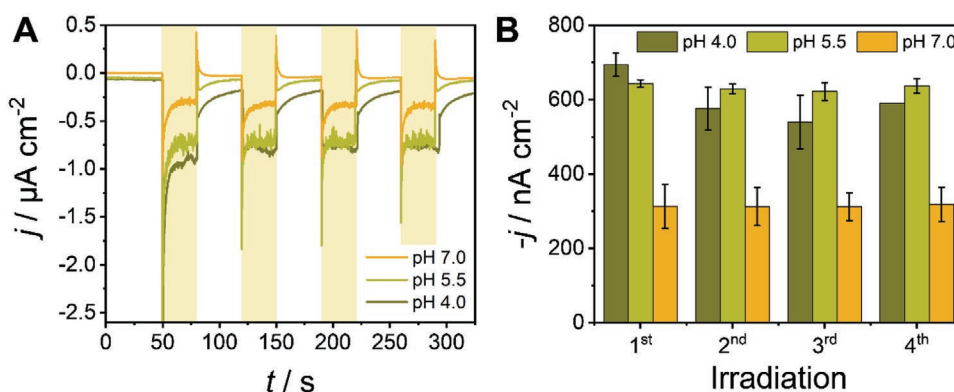
2203232 (5 of 9)

Figure 4. Electrodes integrating PSI–H$_2$ase fusion complexes embedded within the P-Os redox polymer measured at different pH values. A) Representative photoamperometric responses. Au-disc electrode. Ar-saturated buffer. Illumination with red light (43 mW cm^{-2}) during the times indicated by the yellow background. E_{app}: 200 mV versus SHE. B) Summary of results obtained from the photocurrent response at different pH values. Error bars represent the standard deviation ($n = 2$).

case, the photocurrent response under the exclusion of O$_2$ was negligible (Figure S13A, Supporting Information), although the modified film was similarly stable on the electrode surface, as revealed by the P-Os redox signal (Figure S13B, Supporting Information). The observed results confirmed that the photocurrent response obtained before was indeed related to H$_2$ production with the bioelectrode.

The modified electrodes were investigated using scanning photoelectrochemical microscopy (SPECM) to attain direct evidence for photoH$_2$ evolution with the isolated PSI–HoxYH complexes in vitro. SPECM enables the precise positioning of a microelectrode in close proximity to a surface of interest. In addition, focalized illumination of the sample is attained by coupling the light source with the microelectrode acting as an

extended light guide.[18] In order to ensure selective and highly sensitive detection of H$_2$, a hydrogenase-based microbiosensor was used as the SPECM tip probe. The previously developed biosensor consisted of a carbon-based microelectrode modified with a [NiFe]-hydrogenase from *Desulfovibrio vulgaris* Miyazaki F embedded into a viologen-modified redox polymer.[19] Cyclic voltammograms performed with the modified microelectrode under Ar revealed the characteristic wave of the viologen-modified polymer with a midpoint potential of about −270 mV versus SHE (Figure S14, Supporting Information). After the addition of H$_2$ into the electrochemical cell, the appearance of an anodic response confirmed the enzymatic H$_2$ conversion mediated by the viologen-modified redox polymer, thus enabling selective H$_2$ detection with the microbiosensor. It is
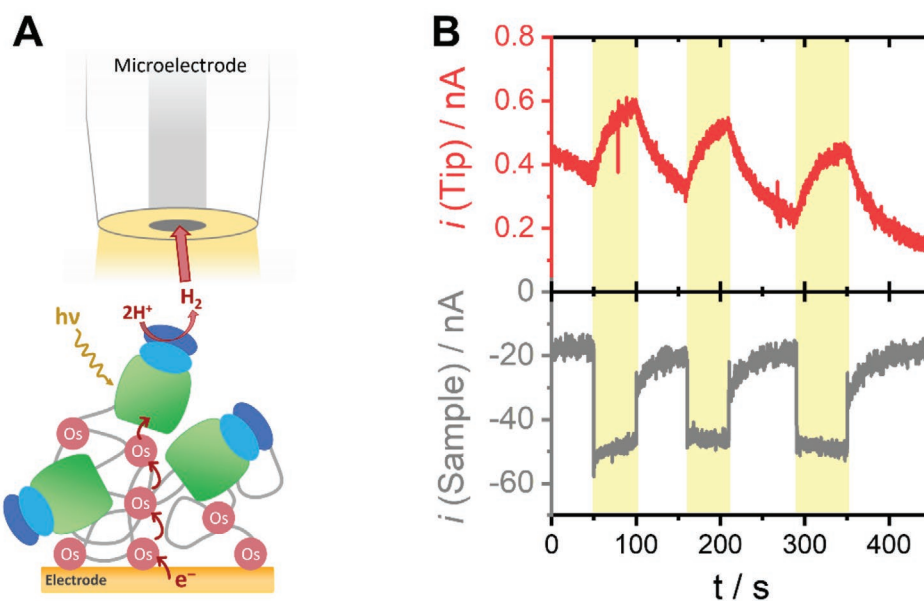

Figure 5. Local detection of photoH$_2$ by SPECM. A) A *Dv*MF[NiFe]-H$_2$ase-modified microelectrode (tip) is used as a probe for the in situ selective detection of H$_2$ evolved during the illumination of a PSI–H$_2$ase fusion complex/P-Os redox polymer-modified electrode (sample). B) Amperometric response recorded at the tip and sample at sequential periods of dark and light. Au-coated Si wafer as substrate. Ar-saturated phosphate-citrate buffer, pH 5.5. Local illumination through the modified microelectrode during the times indicated by the yellow background. E_{app}: 200 mV versus SHE for both electrodes.

© 2023 The Authors. Advanced Energy Materials published by Wiley-VCH GmbH

worth noting that under an Ar atmosphere, H_2 evolution was observed at applied potentials more negative than the midpoint potential of the redox polymer. This process was prevented under a H_2 atmosphere. For sensitive detection of photoH_2, an applied potential of 200 mV versus SHE was selected.

As schematically depicted in **Figure 5**A, the microbiosensor was used as a probe in a SPECM setup for the analysis of an electrode modified with PSI–HoxYH complexes within a P-Os film. The current response at the PSI–HoxYH/P-Os modified electrode and at the microbiosensor were simultaneously monitored while applying subsequent dark and light conditions. The obtained results (Figure 5B) revealed an anodic current response at the microbiosensor associated with an increased cathodic current at the sample every time the electrode was locally illuminated. Because of a larger illuminated area in comparison with the microelectrode size, larger photocurrents were recorded at the PSI–HoxYH/P-Os modified electrode in comparison with the tip microelectrode.[18b] The observed increase in anodic current at the microbiosensor was undoubtedly associated with the selective collection of evolved H_2 under the illumination of the biophotoelectrode.

An additional control experiment was performed by SPECM analysis of electrodes that were modified with isolated PSI monomers extracted from *Thermosynechococcus vestitus* (formerly known as *Thermosynechococcus elongatus*), instead of using PSI–HoxYH complexes. The results obtained in this case are summarized in Figure S15 (Supporting Information) and revealed only a minor photocurrent response at the sample electrode while no noticeable anodic currents were recorded at the H_2 microbiosensor during illumination of the sample. In this case, PSI lacking the H_2ase unit is not able to perform H_2 evolution, and therefore no response was expected. Thus, the obtained results unequivocally confirmed the possibility for light-induced H_2 evolution in vitro with isolated PSI–HoxYH complexes embedded in a redox polymer matrix.

3. Conclusion

After achieving a successful in vivo PSI-hydrogenase fusion protein complex assembly, the subsequent isolation, purification, and integration into an electrode for in vitro photoH_2 production could be demonstrated. This strategy constitutes the first time that an in vivo construct is used for H_2 production in vitro and allows for the straightforward evaluation and optimization of fusion complexes. The obtained results can be used to optimize photoH_2 production both in vivo and in vitro. By shortening the distance between the terminal FeS cluster at PSI and the FeS cluster at the hydrogenase, electron transfer from PSI to H_2ase should be significantly improved. As a result, the isolated PSI–H_2ase fusion complexes can be used for the fabrication of biophotoelectrodes by integrating the protein complexes into a redox polymer matrix for their immobilization and electrical wiring of the electrode surface with the P_{700} site of PSI. Due to the fast kinetics for electron transfer from PSI to H_2ase, ultimately reducing protons from the solution, the possibility of short-circuiting photogenerated high-energy electrons is prevented. Thus, the isolated fusion complexes embedded into the redox polymer film can effectively produce H_2 under

illumination of the modified electrode. Therefore, neither a specific orientation of PSI nor a physical separation between the terminal redox centers at the photosystem are required to prevent short-circuiting of reduced charge carriers.

Interestingly, PsaD–HoxYH produced significantly more photoH_2 in vivo in comparison to PsaE-16–HoxYH. However, in this study, the latter was used for the fabrication of electrodes and photoH_2 production in vitro since it grew better under autotrophic conditions. This facilitated the isolation and purification of adequately assembled and functional PSI–H_2ase complexes. The observation of better in vivo H_2 production with PsaD–HoxYH opens new possibilities for an even improved performance of biophotoelectrodes for H_2 production in vitro. It will be of great interest to compare the performances of different PSI–H_2ase assemblies for their in vivo and in vitro photoH_2 production capabilities.

4. Experimental Section

Construction of Plasmids: All primers used in this study are listed in Table S1 (Supporting Information). The PsaD–HoxYH strain was constructed as described earlier.[2b] For introducing a fusion of HoxY to PsaE first a deletion strain of *psaE* was constructed in the Δ*hoxEFUYH* background. The *psaE* deletion construct (pDPSAE) was made by Gibson assembly whereas the fusion construct (pEY16) was made by TAR-cloning as described earlier.[2b] In this case HoxY was fused with its C-terminus to the N-terminus of PsaE with a 16 amino acid linker.

Generation and Growth of Strains: Wild-type cells and the Δ*hox* were grown at 50 μE m^{-2} s^{-1} on BG-11 agar plates and bubbling cultures. Cells transformed with pDPSAE were grown at 5 μE m^{-2} s^{-1} on plates. After segregation, the Δ*hox*Δ*psaE* strain was grown at 10 μE m^{-2} s^{-1} in air bubbled cultures without glucose and transformed with pEY16. In this case, cells were grown in shaking cultures (100 rpm) for about three days at 5 μE m^{-2} s^{-1} with 10×10^{-3} M glucose before plating them on BG-11 with 10×10^{-3} M glucose and 20 μg mL^{-1} erythromycin. The plates were kept at 5 μE m^{-2} s^{-1} for several weeks before colonies appeared. Segregation of all the resulting strains was either checked by PCR or Southern blotting as described earlier.[2b] Successful transformation in case of the Δ*hox* and the fusion strains was also checked by measuring their hydrogenase activity.

Hydrogen Measurements: Hydrogenase activity was measured in whole cells in the presence of 10×10^{-3} M dithionite and 5×10^{-3} M methyl viologen with a hydrogen electrode as described earlier.[20] Cells were grown under photoautotrophic conditions until they reached a density of OD_{750} of 3. They were used without further treatment for hydrogenase activity measurements.

Protein Extract Preparation, Polyacrylamide Gel Electrophoresis, and Immunoblotting: Samples for protein gels were prepared and used for polyacrylamide gel electrophoresis as described earlier.[2b,21] However, for the fractionation into soluble and membrane samples, the whole cell extract was centrifuged in an ultracentrifuge at 100 000 *g* for 45 min and 4 °C to remove small membrane vesicles from the soluble extract. Accordingly, membranes were washed once in ACA (750×10^{-3} M ε-amino caproic acid, 50×10^{-3} M BisTris/HCl, pH 7.0, 0.5×10^{-3} M EDTA) to minimize soluble protein contamination. In the 1D SDS PAGE immunoblotting analysis, an amount corresponding to 1 μg of Chl were loaded per lane for the membrane samples and 8 μg of protein for the soluble samples. The PsaE antibody was purchased from Agrisera (Umeå, Sweden). 2D BN-SDS PAGE was performed as described earlier.[2b]

Cultivation of Synechocystis sp. PCC 6803 PsaE–HoxYH: Cultures were grown in BG11 medium + 10 mL L^{-1} stock solution 1 (540 μL L^{-1} EDTA, 0.6 g L^{-1} ferric ammonium citrate, 0.6 g L^{-1} citric acid × 1 H_2O, 3.6 g L^{-1} $CaCl_2$ × 2 H_2O), autoclaved separately) at 30 °C and 15 μE m^{-2} s^{-1} white

light with 5% CO_2 supply. The selection was achieved by the addition of 50 µg mL^{-1} kanamycin and 20 µg mL^{-1} erythromycin.

PSI–Hox Purification: *Synechocystis* sp. PCC 6803 PsaE-HoxYH cells were sedimented (30 min, 4 °C, 6000 rpm, JLA 8.1000) and resuspended in washing buffer (20 × 10^{-3} M MES pH 6.5, 10 × 10^{-3} M CaCl$_2$, 10 × 10^{-3} M MgCl$_2$, 500 × 10^{-3} M mannitol). After 90 min of incubation with 0.2% (w/v) lysozyme with agitation at 37 °C in darkness, cells were disrupted via French Press (4 × 1 min at 16 000 psi). Thylakoid membranes and cell debris were washed (30 min, 4 °C, 32 500 rpm, Ti-45) and the sediment was resuspended in extraction buffer (20 × 10^{-3} M HEPES pH 7.5, 10 × 10^{-3} M CaCl$_2$, 10 × 10^{-3} M MgCl$_2$, 500 × 10^{-3} M mannitol) with 0.5% (w/v) lauryldimethylamine oxide (LDAO). The suspension was incubated at 20 °C with slow agitation and in the dark for 30 min, followed by ultracentrifugation (60 min, 4 °C, 42 000 rpm, Ti-70). The supernatant containing solubilized thylakoid membrane proteins was applied on a discontinuous sucrose gradient[15] to remove excess carotenoids and phycobilisomes. Chlorophyll-containing fractions were collected and mixed with ammonium sulfate (AMS) high salt buffer (20 × 10^{-3} M HEPES pH 7.5, 10 × 10^{-3} M CaCl$_2$, 10 × 10^{-3} M MgCl$_2$, 3.38 M (NH$_4$)$_2$SO$_4$) in a ratio of 60:40 sample:AMS, followed by filtration (0.45 µm). Proteins were isolated via hydrophobic interaction chromatography (HIC) at the ÄKTA purifier (GE Healthcare, Sweden). The system and column (HIC POROS 50 OH, 53 mL, Thermo Fisher Scientific, USA) were washed with three column volumes (CV) of HIC equilibration buffer (20 × 10^{-3} M HEPES pH 7.5, 10 × 10^{-3} M CaCl$_2$, 10 × 10^{-3} M MgCl$_2$, 1.65 M (NH$_4$)$_2$SO$_4$, 0.03% (w/v) β-DDM). After application of the sample, the column was washed with two CV of HIC equilibration buffer, before elution by gradually decreasing the AMS concentration to 0 M (NH$_4$)$_2$SO$_4$ over 6 CV. PSI-containing fractions were concentrated (AMICON centrifugal filter unit, MWCO: 100 kDa) and transferred into the final storage buffer (20 × 10^{-3} M MES pH 6.5, 10 × 10^{-3} M MgCl$_2$, 10 × 10^{-3} M CaCl$_2$, 500 × 10^{-3} M mannitol, 0.03% (w/v) β-DDM). Ultimately, free detergent was eliminated via gel filtration using Sephadex G-25 resin (20 min, 4 °C, 10 000 rpm, SS34) in storage buffer, followed by chlorophyll determination via methanol extraction as described elsewhere.[22]

Chemicals and Materials: All chemicals were of laboratory grade or higher and used without further purification. Potassium dihydrogen phosphate, di-potassium hydrogen phosphate trihydrate, and potassium chloride were obtained from VWR Chemicals. Citric acid monohydrate was from J.T. Baker. Tris-HCl was purchased from AppliChem. Magnesium chloride was from Carl Roth. Poly(ethylene glycol)diglycidyl ether (PEGDGE, M_n = 400 g mol^{-1}) was from Polysciences. Methyl viologen dichloride hydrate (MV^{2+}) and bovine serum albumin (BSA) were from Sigma-Aldrich. A detailed description of the synthesis and purification of the redox polymer poly(1-vinylimidazole-*co*-allylamine)-[Os(2,2′-bipyridine)$_2$Cl]Cl (P-Os) can be found elsewhere.[23] All solutions were prepared using deionized water (ρ = 18 MΩ cm) from a water purification system (SG Water).

Fabrication of Modified Bioelectrodes: Au-modified wafers were obtained by coating Si(100) wafers (Wacker) with titanium (adhesion layer) and gold using a metal vaporization setup. Prior to use, the Au-coated wafers were cut to the desired size, cleaned using Piranha solution (concentrated H$_2$SO$_4$ and 30 wt% H$_2$O$_2$ in a 3 to 1 volumetric ratio), rinsed thoroughly, and dried under an Ar stream.

Au disc electrodes (2 mm diameter, CH Instruments) were polished using diamond suspensions (LECO) of decreasing particle sizes (0.3, 0.1, and 0.05 µm) and subsequently sonicated in ethanol and deionized water for 2 min. Afterward, the electrodes were electrochemically cleaned by cyclic voltammetry in 0.5 M H$_2$SO$_4$ (15 cycles at 100 mV s^{-1} between −0.2 and 1.6 V vs Ag/AgCl/3 M KCl).

The electrode surface was modified with 2.5 µL of a mixture of the purified PSI–H$_2$ase construct (0.135 mg$_{Chl}$ mL^{-1}), P-Os (2.5 mg mL^{-1}), and PEGDGE (0.04 mg mL^{-1}). The modified electrodes were incubated overnight at 4 °C in the dark. Before measurement, an additional incubation was performed for 30 min in 50 × 10^{-3} M Tris-HCl buffer solution of pH 9.0 (containing 100 × 10^{-3} M KCl, 10 × 10^{-3} M MgCl$_2$, and 10 × 10^{-3} M CaCl$_2$) to induce polymer collapse and crosslinking.[17]

For control measurements, PSI monomers from *T. vestitus* (formerly *T. elongatus*) isolated and purified as described elsewhere[7,15] were employed, using the same *Chl* loading as for PSI–H$_2$ase constructs during electrode modification. Additionally, electrodes modified with BSA (0.5 mg mL^{-1}) embedded in a P-Os (2.5 mg mL^{-1}) redox polymer matrix were also used.

Electrochemical Characterization of Individual Bioelectrodes: A three-electrode setup was used, comprised of the modified electrode as the working electrode, a Pt mesh as the counter electrode, and Ag/AgCl/3 M KCl as the reference electrode. Measurements under the exclusion of O$_2$ were performed by initially flushing the electrochemical cell with Ar and maintaining an Ar atmosphere during the measurements. As electrolyte solution, Ar-saturated 150 × 10^{-3} M phosphate-citrate buffer was used. The modified electrodes were investigated by performing cyclic voltammetry and photoamperometric measurements using a PGU-BI 100 potentiostat (IPS Jaissle). A He–Xe lamp (LC8 type 03, Hamamatsu Photonics) was used for illumination of the modified electrodes integrating a red foil filter (LEE filters), which provided red light (λ > 600 nm) at an incident power of 43 mW cm^{-2}. All measurements were performed at room temperature.

Local PhotoH$_2$ Detection: In situ local detection of photogenerated H$_2$ was performed by means of scanning photoelectrochemical microscopy (SPECM) using a H$_2$ microbiosensor as described previously.[19] Briefly, a carbon paste microelectrode was modified by drop-casting 5 × 1 µL of a mixture of [NiFe]-hydrogenase from *Desulfovibrio vulgaris* Miyazaki F (100 × 10^{-6} M, *Dv*MF[NiFe]-H$_2$ase) and a viologen-modified redox polymer (poly(3-azidopropyl methacrylate-*co*-butyl acrylate-*co*-glycidyl methacrylate)-viologen, 6.5 mg mL^{-1}).[24] The modified microelectrode was incubated overnight at 4 °C. For H$_2$ detection, the microelectrode was coupled to the lamp used as light source using an optical fiber, enabling localized sample illumination. Before use, a potential of −800 mV versus Ag/AgCl/3 M KCl was applied to the H$_2$ase-modified microelectrode for 120 s to ensure enzyme reactivation.

Supporting Information

Supporting Information is available from the Wiley Online Library or from the author.

Acknowledgements

Conflict of Interest

The authors declare no conflict of interest.

Data Availability Statement

The data that support the findings of this study are available from the corresponding author upon reasonable request.

[1] K. E. Redding, J. Appel, M. Boehm, W. Schuhmann, M. M. Nowaczyk, I. Yacoby, K. Gutekunst, *Trends Biotechnol.* **2022**, *40*, 1313.

[2] a) A. Kanygin, Y. Milrad, C. Thummala, K. Reifschneider, P. Baker, P. Marco, I. Yacoby, K. E. Redding, *Energy Environ. Sci.* **2020**, *13*, 2903; b) J. Appel, V. Hueren, M. Boehm, K. Gutekunst, *Nat. Energy* **2020**, *5*, 458.

[3] a) M. Ihara, H. Nishihara, K.-S. Yoon, O. Lenz, B. Friedrich, H. Nakamoto, K. Kojima, D. Honma, T. Kamachi, I. Okura, *Photochem. Photobiol.* **2006**, *82*, 676; b) H. Krassen, A. Schwarze, B. Friedrich, K. Ataka, O. Lenz, J. Heberle, *ACS Nano* **2009**, *3*, 4055.

[4] C. E. Lubner, P. Knörzer, P. J. N. Silva, K. A. Vincent, T. Happe, D. A. Bryant, J. H. Golbeck, *Biochemistry* **2010**, *49*, 10264.

[5] a) W. M. Schluchter, J. Zhao, D. A. Bryant, *J. Bacteriol.* **1993**, *175*, 3343; b) C. T. Nomura, S. Persson, G. Shen, K. Inoue-Sakamoto, D. A. Bryant, *Photosynth. Res.* **2006**, *87*, 215.

[6] P. Wang, F. Zhao, A. Frank, S. Zerria, A. Lielpetere, A. Ruff, M. M. Nowaczyk, W. Schuhmann, F. Conzuelo, *Adv. Energy Mater.* **2021**, *11*, 2102858.

[7] P. Wang, A. Frank, F. Zhao, J. Szczesny, J. R. C. Junqueira, S. Zacarias, A. Ruff, M. M. Nowaczyk, I. A. C. Pereira, M. Rögner, F. Conzuelo, W. Schuhmann, *Angew. Chem., Int. Ed.* **2021**, *60*, 2000.

[8] R. A. Marcus, N. Sutin, *Biochim. Biophys. Acta* **1985**, *811*, 265.

[9] C. C. Page, C. C. Moser, X. Chen, P. L. Dutton, *Nature* **1999**, *402*, 47.

[10] T. Malavath, I. Caspy, S. Y. Netzer-El, D. Klaiman, N. Nelson, *Biochim. Biophys. Acta Bioenerg.* **2018**, *1859*, 645.

[11] Y. Shomura, M. Taketa, H. Nakashima, H. Tai, H. Nakagawa, Y. Ikeda, M. Ishii, Y. Igarashi, H. Nishihara, K. S. Yoon, S. Ogo, S. Hirota, Y. Higuchi, *Science* **2017**, *357*, 928.

[12] X. Chen, J. L. Zaro, W. C. Shen, *Adv. Drug Delivery Rev.* **2013**, *65*, 1357.

[13] H. Kubota-Kawai, R. Mutoh, K. Shinmura, P. Sétif, M. M. Nowaczyk, M. Rögner, T. Ikegami, H. Tanaka, G. Kurisu, *Nat. Plants* **2018**, *4*, 218.

[14] J. H. Artz, M. Tokmina-Lukaszewska, D. W. Mulder, C. E. Lubner, K. Gutekunst, J. Appel, B. Bothner, M. Boehm, P. W. King, *J. Biol. Chem.* **2020**, *295*, 9445.

[15] O. Çoruh, A. Frank, H. Tanaka, A. Kawamoto, E. El-Mohsnawy, T. Kato, K. Namba, C. Gerle, M. M. Nowaczyk, G. Kurisu, *Commun. Biol.* **2021**, *4*, 304.

[16] C. Eckert, M. Boehm, D. Carrieri, J. Yu, A. Dubini, P. J. Nixon, P.-C. Maness, *J. Biol. Chem.* **2012**, *287*, 43502.

[17] T. Kothe, S. Pöller, F. Zhao, P. Fortgang, M. Rögner, W. Schuhmann, N. Plumeré, *Chem. – Eur. J.* **2014**, *20*, 11029.

[18] a) F. Conzuelo, K. Sliozberg, R. Gutkowski, S. Grützke, M. Nebel, W. Schuhmann, *Anal. Chem.* **2017**, *89*, 1222; b) F. Zhao, N. Plumeré, M. M. Nowaczyk, A. Ruff, W. Schuhmann, F. Conzuelo, *Small* **2017**, *13*, 1604093.

[19] F. Zhao, F. Conzuelo, V. Hartmann, H. Li, S. Stapf, M. M. Nowaczyk, M. Rögner, N. Plumeré, W. Lubitz, W. Schuhmann, *Biosens. Bioelectron.* **2017**, *94*, 433.

[20] K. Gutekunst, D. Hoffmann, U. Westernströer, R. Schulz, D. Garbe-Schönberg, J. Appel, *Sci. Rep.* **2018**, *8*, 6083.

[21] H. Schägger, G. von Jagow, *Anal. Biochem.* **1991**, *199*, 223.

[22] R. J. Porra, W. A. Thompson, P. E. Kriedemann, *Biochim. Biophys. Acta Bioenerg.* **1989**, *975*, 384.

[23] F. Conzuelo, N. Marković, A. Ruff, W. Schuhmann, *Angew. Chem., Int. Ed.* **2018**, *57*, 13681.

[24] a) F. Zhao, P. Wang, A. Ruff, V. Hartmann, S. Zacarias, I. A. C. Pereira, M. M. Nowaczyk, M. Rögner, F. Conzuelo, W. Schuhmann, *Energy Environ. Sci.* **2019**, *12*, 3133; b) J. Szczesny, N. Marković, F. Conzuelo, S. Zacarias, I. A. C. Pereira, W. Lubitz, N. Plumeré, W. Schuhmann, A. Ruff, *Nat. Commun.* **2018**, *9*, 4715.